Synergistic effects of conductivity and cell-imprinted topography of chitosan-polyaniline based scaffolds for neural differentiation of adipose-derived stem cells

Behnaz Sadat Eftekhari[1,2], Mahnaz Eskandari[1]*, Paul Janmey[2]*, Ali Samadikuchaksaraei[3,4,5], Mazaher Gholipurmalekabadi[3,4]

[1] Department of Biomedical Engineering, Amirkabir University of Technology, Tehran, Iran.

[2] Department of Physiology and Institute for Medicine and Engineering, University of Pennsylvania, Philadelphia, PA, USA.

[3] Cellular and Molecular Research Centre, Iran University of Medical Sciences, Tehran, Iran

[4] Department of Tissue Engineering & Regenerative Medicine, Faculty of Advanced Technologies in Medicine, Iran University of Medical Sciences, Tehran, Iran.

[5] Department of Medical Biotechnology, Faculty of Allied Medicine, Iran University of Medical Sciences, Tehran, Iran.

***Corresponding authors:**

Dr. Mahnaz Eskandari

Assistant Professor, Amirkabir University of Technology, 424 Hafez Ave, Tehran, 15875-4413, IRAN

Tel: (+98 21) 6454 23 62;

E-mail: Eskandarim@aut.ac.ir

Prof. Paul A. Janmey

Professor of Physiology, Member, Pennsylvania Muscle Institute, University of Pennsylvania, 1010 Vagelos Research Laboratories, 3340 Smith Walk, Philadelphia, PA 19104-6383

Office: 215 573-7380
Fax: 215 573-6815

E-mail: janmey@mail.med.upenn.edu

Abstract

Smart nano-environments that mimic the stem cell niche can guide cell behavior to support functional repair and regeneration of tissues. The specific microenvironment of nervous tissue is composed of several physical signaling factors, including proper topography, flexibility, and electric conductance, to support the electrical conduction of neuronal communication. In this study, a cell-imprinting technique was used to obtain a hierarchical topographical conductive scaffold based on chitosan-polyaniline (PANI) hydrogels for directing the neural differentiation of rat adipose-derived stem cells (rADSCs). A chitosan-polyaniline hydrogel was synthesized, followed by characterization tests, such as Fourier transform infrared spectroscopy (FTIR), electrical conductivity, Young modulus, and contact angle measurements. A chitosan-PANI scaffold with a biomimetic topography was fabricated by molding it on a chemically fixed culture of PC12 cells. This substrate was used to test the hypothesis that the PC12 cell-imprinted chitosan-PANI hydrogel provides the required hierarchical topographical surface to induce neural differentiation. To test the importance of spatial imprinting, rADSCs were seeded on these conductive patterned substrates, and the resulting cultures were compared to those of the same cells grown on flat conductive chitosan- polyaniline, and flat pure chitosan substrates for evaluation of adhesion, cell viability, and expression of neural differentiation markers. The morphology of rADSCs grown on conductive patterned scaffolds noticeably was significantly different from that of stem cells cultivated on flat scaffolds. This difference suggests that the change in cell and nuclear shape imposed by the patterned conductive substrate leads to altered gene expression and neural differentiation of cultured cells. In addition, the percentage of rADSCs that differentiated into neural-like cells was almost 80 % on the imprinted chitosan-PANI scaffold. In summary, a conductive chitosan-polyaniline scaffold with biomimetic topography demonstrates a promising method for enhancing the neural differentiation of rADSCs for the treatment of neurodegenerative diseases.

Keyword: biomimetic, hierarchical topography, conductive scaffold, stem cells, neural differentiation, cell-imprinted substrate

1. Introduction

The human nervous system consists of the central nervous system (CNS) and the peripheral nervous system (PNS), which play distinct and critical roles in all physiological processes, including recognition, sensory and motor functions of cells [1-2]. Neurodegenerative disorders in the region of the brain and spinal cord, traumatic injuries, and stroke influence the quality life of 2 million people in the United States of America (USA) each year, and this number annually grows by an estimated 11000 cases [3-4]. The regeneration of injured neurons is limited under normal conditions due to two main factors: post-damage scar formation and unguided axonal regrowth [5]. The nerve injury activates the proliferation of glial cells, known as astrocytes in CNS and Schawnn cells (SCs) in the PNS, which create scar tissue and prevent the regrowth of severed axons by producing inhibitory molecules [6] and altering the extracellular environment. Due to the ineffectiveness of numerous strategies for the regeneration of neural defects, full recovery of damaged nerves remains challenging [7].

New studies have also demonstrated the potential of stem cells for the treatment of catastrophic diseases such as neurodegenerative diseases and cancer [8-9]. The stem cell environment (niche) controls the natural regeneration of damaged tissue through providing biochemical (e.g., growth factors and other soluble factors) as well as biophysical cues (e.g., shear stress, elastic modulus, stiffness, geometry, and conductivity). Due to disappointing clinical results of therapeutic approaches with growth factors alone (e.g., angiogenic factors), fabrication of engineered scaffolds with appropriate biophysical and biochemical properties have been proposed [10-12].

Fundamental developments in tissue engineering have made strides to control stem cell behaviors such as proliferation, migration, and differentiation by applying biophysical signals [13]. In particular, nerve tissue engineering scaffolds must present appropriate physical characteristics supplying the proper topography, mechanical elasticity, and electrical conductivity to accelerate axonal growth during regeneration [14]. Micro and nano topographical substrates can actuate the mechano-transduction pathways that regulate stem cell fate by contact guidance through the rearrangement of cytoskeleton alignment, leading to changes in nucleus shape and altering gene expression [15].

Most studies have indicated that nanopatterned surfaces activate cell surface proteins such as integrins, which are responsible for cell surface signal transduction, cluster assembly, and formation of focal adhesion complexes containing vinculin, paxillin, and focal adhesion kinase (FAK), which alter the arrangement and mechanical tension of the cytoskeleton [16-17]. Ultimately, the mechanotransduction pathway activated by mechanical tension changes the nucleus shape and the expression profile of genes involved in stem cell differentiation [18]. Since the stem cell niche comprises nano and micropatterned topographies, scaffolds with various geometries such as continuous topography, discontinuous topography and random topography with different spatial dimensions ranging from nanometers to micrometer (which are typically fabricated by photolithography, microcontact printing, microfluidic patterning, and electrospinning techniques) are utilized for regulation of stem cell fate to neural differentiation [19-20]. Despite much progress to attain precise control of stem cell behavior using engineered patterned substrates, high yield, reliable, safe, and cost-effective control of stem cell fate remains a challenge.

In 2013, Mahmoudi et al. reported the cell imprinting method as a repeatable, valid, and cost-effective procedure for controlling stem cell fate [21]. In this method, a hierarchically patterned substrate (HPS) was obtained by molding substrates on a surface containing chemically fixed cells as a template to mimic the cell shape [22]. In a recent survey, PDMS substrates with Schwann cell-like topographies were utilized to induce Schwann cell-like differentiation of adipose-derived mesenchymal stem cells (ADSCs) [23]. Furthermore, cell shape topography can act as a powerful regulator of cell behavior such as adhesion, differentiation, growth.

In addition to the role of substrate topography, conductive scaffolds that mimic the electrical conductivity of native tissue promote stem cell plasticity and differentiation into specific lineages by altering their membrane depolarization [24]. Because of the involvement of endogenous electrical signals in neurogenesis, nerve growth, and axon guidance, biophysical studies of electrical signals are increasingly used to direct stem cell differentiation toward neuron-like cells [25]. Electrically conducting polymers such as polypyrrole, polyaniline (PANI), polythiophene, and their derivatives (mainly aniline oligomers and poly (3,4-ethylene dioxythiophene)) are bioactive biomaterials for controlled delivery of electrical signals to cells [26]. Despite the biocompatibility of these polymers, their weak mechanical properties and poor processability require blending these polymers with other biomaterials [26]. Chitosan (CS), as a biocompatible, biodegradable,

non-immunogenic, and antibacterial biomaterial, is frequently considered a promising candidate for electroactive hydrogel fabrication [27-29]. Hence, we proposed to examine potential synergetic effects of cell-imprinted conductive CS-PANI hydrogels on the differentiation of rat adipose-derived stem cells (rADSCs) into neuron-like cells. In the present *in vitro* study, we synthesized pure CS and conductive CS- PANI hydrogels. In the next step, a chemically fixed differentiated culture of PC12 cell was employed as a template on which the conductive hydrogel was cast. After the removal of the remaining cells/debris, the conductive scaffold was obtained with the specific topography of the cells that were used as a template. Consequently, the potency of the cell-imprinted conductive scaffold and a control flat conductive scaffold was investigated for inducing the neural differentiation of rADSCs.

2. Materials and methods

2.1 Materials

Polyaniline (PANI, emeraldine base, Mw 65,000), chitosan (%DD=80, medium molecular weight), and 3-(4,5-dimethylthiazol-2-yl)-2,5-diphenyl tetrazolium bromide (MTT) were purchased from Sigma-Aldrich. Glutaraldehyde (50% w/w, analytical grade) and paraformaldehyde were acquired from Fluka. AR grade chemicals of N-methyl-2-pyrrolidone (NMP), acetic acid, and methanol were used as received.

2.2 Fabrication of flat and cell-imprinted CS-PANI substrates

2.2.1 Preparation of CS-PANI blend hydrogels

A 1 wt% solution of CS was prepared by dissolving chitosan in 2% acetic acid with vigorous stirring. In order to crosslink the chitosan chains, 0.01 mole% of glutaraldehyde was added into the solution, and the mixture stirred for 1h. PANI was dissolved in N-methyl-2-pyrrolidone (NMP) to obtain a 0.5 wt% solution. In order to create a blend of chitosan-polyaniline with 2.5% (wt%) PANI, the desired amount of PANI/NMP solution was mixed with the chitosan solution. Then the mixture was stirred at room temperature for 12 h [30].

2.2.2 PC12 cell culture and differentiation

PC12 cells were seeded on 6-well plates coated with poly-D-lysine (PDL) and laminin (Lam) in Gibco™ 1640 Roswell Park Memorial Institute (RPMI) medium with 10% horse serum (HS), 5 % fetal bovine serum (FBS) (Seromed, Germany) and 1% penicillin- streptomycin (Sigma, USA). After 24 hours, the medium was replaced with serum-free medium containing 100 ng/ml nerve growth factor (NGF) (GeminiBio, USA) and maintained at 37˚C in a 95% humidified incubator with 5% CO_2 [31]. The medium of cells was changed every 2 days until they reached 80% confluency. The cells were fixed with 4% paraformaldehyde (PFA) in phosphate buffered saline (PBS) (Sigma, USA) (pH= 7.4) for 2h at 25 °C before treatment to preserve their shape during the printing process.

2.2.3 Fabrication of flat and PC12 cell-imprinted conductive substrates

The prepared pure CS and CS-PANI hydrogels were poured on the fixed cell samples and incubated to dry at 37 °C for 48 h. Flat CS and flat conductive CS-PANI substrates were fabricated by casting them on glass in order to distinguish the specific effect of surface topography from scaffold conductivity on cell behavior. The flat and cell-imprinted substrates were removed from the residues of solvent and cell debris by washing them with 1M NaOH solution after molding, and a UV light was used for sterilization. The total mass, temperature, and time of curing were the same for all prepared scaffolds.

2.3 Characterization of prepared substrate

2.3.1 Fourier-transform infrared spectroscopy (FTIR) spectra

A Thermo Nicolet Nexus FTIR spectrometer in the transmittance mode at 32 scans with a resolution of 4 cmK was used for recording the FTIR spectra of chitosan and the blend samples. Spectra in the frequency range of 4000– 400 cm^{-1} were measured using a deuterated tri-glycerine sulfate detector (DTGS) with a specific detectivity of $1*10^9$ cm Hz1/2 wK1.

2.3.2 Imaging

The surface morphology of the topographical substrates and flat substrates was investigated by scanning electron microscopy (SEM) (Hitachi Japan; apparatus working at 10 keV accelerating voltage), atomic force microscopy (AFM; DME DS 95Navigator 220) and optical microscopy

(Nikon Optiphot 200). Before SEM imaging, all samples were coated with a thin layer of gold using a sputtering machine. AFM contact mode was performed using a rectangular cantilever (HQ:NSC18/Al BS, MikroMasch, Bulgaria) with a spring constant of 2.8 N/m and a conical tip of 8 nm radius. The surface of the sample up to 90 μm^2 was scanned by a scan rate of 0.05 Hz and setpoint force 0.5 nN. The standard software of the instrument (JPKSPM Data Processing) was utilized for image analysis.

2.3.3 Electrical conductivity

The electrical conductivity of fabricated substrates was measured by applying a two-point probe method (Keithley, model 7517A). The electrical conductivity (σ) is obtained as the inverse of resistivity. The resistivity of three samples from each group of the substrate was measured by passing a constant current through the outer probes and recording the voltage via the inner probes. The resistivity of samples was calculated as follows:

$$\rho = \frac{\pi}{ln2}(\frac{V}{I})\mathrm{t}$$

where: I, V, and t indicate the applied current, voltage, and the sample thickness (200 μm), respectively [32].

2.3.4 Mechanical test

The substrates were immersed in PBS to reach the equilibrium swelling before performing mechanical tests. The mechanical properties of all fabricated samples were determined using AFM. A Molecular Imaging Agilent Pico Plus AFM system (now known as AFM5500 Keysight technologies) with silicon nitride probes and 5 μm spherical (nominal value) tips (CP-PNPL-BSG, and a spring constant of $0.08 Nm^{-1}$ was used to measure the Young's modulus of samples.

2.3.5 Contact angle

The static (sessile drop) water contact angle of the prepared substrates was assessed using a contact angle apparatus (DSA20, Germany) at room temperature. A droplet of ultra-pure water was placed on the fixed sample surface, and the measurement was performed 3 s after equilibration. Then, a camera recorded the water contact angle of each surface. This

measurement was repeated at three or more different locations on each sample to calculate the average value of the contact angle.

2.3.6 Degradation rate

The in vitro degradation of substrates was followed for 5 weeks in PBS (pH =7.4) at 37 °C. Three samples from each group with ∼40 mg weight were immersed in 10 ml of PBS at pH = 7.4 and 37°C. At time points of 3, 7, 10, 14, 21, and 30 days, each of the samples was taken out and dried for 12h after surface wiping, and its weight was recorded. The following equation was used for the calculation of sample weight loss:

Degradation (%) = $(W_0 - W_d)/W_0 \times 100\%$

Where W_0 is the dry weight of the sample at time t = 0 and W_d is the dry sample weight after removal from the solution. The pH values of the solutions during scaffold immersion were also recorded.

2.4 CS-PANI substrates / rADSCs interaction

2.4.1 Isolation and Culture of rat Adipose-derived Stem Cells (rADSCs)

Rat adipose-derived stem cells (rADSCs) were isolated and expanded by a procedure described in a published study [33]. In brief, subcutaneous adipose tissue samples were isolated by needle-biopsy aspiration according to a previously published methodology. DMEM medium (GIBCO, Scotland) containing 10% (v/v) FBS and penicillin (100 IU/ml)-streptomycin (100 µg/ml) was used for transportation to the cell culture laboratory. After washing the tissue sample with DMEM-based buffer three times, the samples were gently cut into small pieces and incubated with 0.05 mg/ml collagenase type I (Sigma, USA) for one 1h to digest the epididymal fat. The separated cells were collected from the resulting suspension after centrifugation at 200 ×g for 5 minutes. The rADSCs were resuspended in DMEM supplemented with 10% FBS, 100 U/mL penicillin and, 100µg/mL streptomycin in an incubator (37°C, 5% CO2). The culture medium was changed to remove non-adhered cells and debris.

2.4.2 Characterization of rADSCs by flow cytometry and immunocytochemistry.

The rADSCs were examined by flow cytometry for identification of surface markers. The cells were identified for expression of mesenchymal markers such as CD29 and CD90 and the

hematopoietic markers CD34 and CD45 (all antibodies obtained from Novus Biologicals company, US). Briefly, 1×10^6 cells in PBS were incubated with 1 μg of each antibody for 1 hour and then washed with PBS for 3 times. Ultimately, cells were treated with secondary antibodies and protected from light for 30 minutes. All cell preparations were analyzed by flow cytometry (FACSCalibur, BD), and data analysis was performed with FlowJo software (Tree Star). The rADSCs were also characterized by immunocytochemical staining as follows: the cells were fixed with 4% PFA in PBS for 15 min and permeabilized with 0.25% Triton X-100 in PBS for 10 min at RT. 3% BSA as blocking solution was added to samples for 30 min and incubated with the primary antibodies (diluted block solution) overnight at 4 °C. Fluorochrome-conjugated secondary antibodies were then added to samples for 1 h at RT and DAPI solution for another 10 min to stain the nucleus. Finally, the sample was rinsed with PBS 3 times. Fluorescence signals were detected using a Leica DMIRE2 microscope under the proper exciting wavelength.

2.4.3 Stem Cell Seeding on cell-imprinted substrates

The prepared substrates were placed into the 6-well plates. rADSCs (3×10^3 cells/cm^2) were then cultured on the conductive cell-imprinted substrates, conductive flat substrates, and flat pure chitosan films. After 24 h, 600 μL/cm^2 of fresh DMEM with 10% (v/v) FBS was added to each well to cover the substrates completely.

2.4.4 Cell Viability

The viability of rADSCs cells was investigated by an MTT assay. To perform this test, a cell density of 2×10^4 cells/cm^2 were cultured on flat and cell- imprinted CS and CS-PANI substrates for 1 day, 3 days, 7 days and 14 days in the incubator (37°C, 5% CO2). At these specified times, the cells were washed with PBS, and then the MTT solution was added into well. After incubation for 4 h, live cells created formazan crystals and were washed with PBS. ADMSO/isopropanol solution was added to dissolve the crystals. Finally, the Optical Density (OD) was measured using a spectrophotometer at a wavelength of 570 nm. The following formula determined the absorbance value:

Absorbance value (OD) = Average OD of the samples – Average OD of the negative control

All data of the test were expressed as means ± standard deviation (SD) for n = 4. The Kolmogorov–Smirnov test was applied to investigate the normal distribution of each group of

samples. Finally, a one- way ANOVA and Duncan test (GraphPad Prism 7 software) was performed to compare the data. $P<0.05$ was considered a significant difference.

2.4.5 F-actin staining

Cell morphology and attachment on scaffolds were evaluated through F-actin staining. The ADSCs were cultured on different substrates at 5000 cells/cm^2. After 72 hours, cells were rinsed with 1x PBS, fixed with 4% PFA and permeabilized with 0.1% Triton X-100. After rinsing with PBS three times, Alexa- Fluor 647 phalloidin (Invitrogen) and DAPI staining (Sigma) were added to samples for 1 hour in the dark. Cells were observed and photographed under an inverted fluorescence microscope (Eclipse Ti-S, Nikon).

2.4.6 Neural lineage induction

The rADSCs of the 4th passage were seeded on a six-well culture plate at a density of 5×10^5 cell/ml with 1 ml of neurosphere medium containing serum-free DMEM/F12 with 2 % B27 supplement (Thermo Fisher, USA) and 20 ng/ml of basic fibroblast growth factor (bFGF) (Thermo Fisher, USA) for 3 days. The neurospheres were seeded on the 6-well plate and cultured in the neurosphere medium containing 5% FBS. After 2 days, the cells were trypsinized by trypsin/EDTA (0.05 % trypsin/ 0.5 mM EDTA) and seeded on substrates in a 24-well plate. The cell suspension containing 1×10^5 cell/ml density was added to the top of the plate. The 3D culture was promoted in the neurosphere medium containing retinoic acid (0.1 M) for five days.

2.4.6.1 Immunostaining

The cell morphology and expression of neuron cell-specific markers were investigated using optical and fluorescence microscopy (Nikon, Japan) to evaluate the neural differentiation capability of rADSCs on prepared substrates. After 8 days from neural induction, the cells seeded on substrates were rinsed with PBS and fixed with 4% PFA in PBS (pH 7.4) for 20 min. In the next step, the cells were permeabilized in a solution containing 0.5% Triton X-100 in PBS for 10 min. To block non-specific antibodies, the cells were incubated with 10% normal goat serum for 1 h at room temperature (0.05% Tween 20 and 1% (w/v) bovine serum albumin (BSA)). Detection and characterization of neuronal cells were carried out by staining the cells with antibodies against GFAP and MAP2. Antibodies to GFAP (1:100; Abcam) and MAP 2 (1:50; Millipore) were added to the cell medium for staining overnight at 4°C. After cells were

washed with PBS, the secondary antibody, including Alexa 488-conjugated goat anti-mouse and anti-rabbit antibodies, was added to cells and incubated for 1h. Finally, the nuclei of cells were counterstained with DAPI. Fluorescence images were taken by an Olympus BX51 fluorescence microscope.

2.5 Statistical analysis

Statistical analyses were performed using SPSS. Data are expressed as the mean – SD, and $p < 0.05$ was considered statistically significant.

3. Results

3.1 Study design

In the current study, differentiation of rADSCs to neural lineage cell is reported using conductive CS-PANI substrates with imprinted PC12-like topography. **Figure 1** represents the method of this study. First, CS-PANI based hydrogels was prepared as well as PC12 cells were differentiated into neural cells using NGF. After the fixation of these cells, conductive CS-PANI substrate with PC12 morphologies were prepared by mold casting. These substrates were characterized with FTIR assay and SEM and AFM imaging. Also, the electrical conductivity, Young's modulus, wettability and degradation rate of prepared scaffolds were evaluated. In the next step, stem cells were isolated from rat adipose tissue and identified for expression of mesenchymal markers using flow cytometry and immunostaining. The rADCSs were cultured on the flat and patterned CS-PANI substrates. In next step, F- acting staining and AFM imaging were used to examine rADSCs attachment and morphology on the substrates. Ultimately, the neural differentiation of rADSCs was evaluated after 8 days by immunostaining.

3.2 Characterization of CS-PANI substrates

3.2.1 Fourier-transform infrared spectroscopy (FTIR) spectra

The FTIR spectra of pure chitosan and PANI/CS blend substrates are shown in **Figure 2**. In the pure chitosan spectrum, the quite broad peak at 3320 cm^{-1} can be assigned to the overlapping of OH and NH2 stretches. The bands occurring at 2918 cm^{-1} and 2873 cm^{-1} are ascribed to the C-H stretching of the aliphatic group. The transmission peaks at 1660 cm^{-1} belong to the C=O in

amide groups (NHCOCH3) because of the partial deacetylation of CS. N-H bending was observed at 1554 and 1416 cm^{-1}. The transmission peak at 1386 cm^{-1} is due to the C-OH vibration of the alcohol groups in CS. Other main peaks observed in CS spectra involving 1299 cm^{-1}, 1254 cm^{-1}, and 1144 cm^{-1} are ascribed to anti-symmetric stretching of the C-O-C bridge and the C-O stretching, respectively [34-35]. After blending PANI with CS, a small shift of peaks can be seen for PANI–CS composite with N–H stretching vibrations at 3290 cm^{-1}, C–H stretching and vibrations at 2887/2861cm^{-1}, respectively. A slight shift of peaks was also indicated with the amide I and II vibrations at 1646 cm^{-1} for CS-PANI composite. Because of interactions between chitosan and polyaniline and conformational changes, small shifts occurred on the C–H bending vibration of the amide methyl group (1386 cm^{-1}) and the C–O stretching vibrations at 1161- 1034 cm^{-1}. The characteristic transmission bands of PANI were also authenticated in the CS-PANI blend spectrum. The transmission peaks corresponding to the C=N stretching vibration of the quinonoid ring and the C=C stretching vibration of the benzenoid ring can be seen at 1554/1519 cm^{-1}, respectively [36-37]. The presence of these peaks confirms that the synthesized composite samples contained PANI.

3.2.2 Microscopic observation

As shown in **Figure 3(a)**, PC 12 cells immediately after plating have small and rounded shapes. The morphology of NGF-induced differentiation of PC12 cells is shown in **Figure 3(b)**. The differentiation of PC12 cells into neuron-like cells leads to the outgrowth of neurites [31]. Analysis of the optical images demonstrated that the PDL/Lam coatings and NGF supported PC12 cell attachment and differentiation, respectively, as evidenced by the presence of neurite outgrowth. The color of pure PANI is dark green; the visible feature of CS-PANI blends was a uniform dark green color. Therefore, the morphology of blend substrates was not optimal for optical microscopy. The surface morphology of flat substrates and PC12-imprinted substrates was investigated using SEM imaging. As shown by SEM (**Figure 3c-d**), the pure CS films showed a homogeneous and smooth surface, and after adding PANI the smoothness of substrates is approximately preserved. Also, to evaluate the PC12- printed pattern on pure CS and CS-PANI blends, SEM images were obtained from these substrates. SEM and AFM micrographs of a PC12-imprinted substrate is shown in **Figure 3 (e-f)** and **Figure 3(g)**. The replicated shapes on the substrates are similar to the morphology of PC12 cells. The transferred topography on

pristine CS and CS-PANI substrates mimics the large body and the network of neurites of differentiated PC12 cells. Also, the AFM height profiles (**Figure 3(h))** of the PC12 cells-imprinted revealed that surface topography had the same shape and depth as cultured PC12 cells.

3.2.3 Electrical conductivity

Figure 4(a) illustrates the electrical conductivity of all prepared substrates. The conductivity of the substrates was increased from 7.5×10^{-8} to 10^{-4} S/cm by enhancing the amount of PANI from 0 to 2.5 wt. % ($P \leq 0.0001$). The conversion of the emeraldine base to the emeraldine salt form of PANI occurs by doping with acetic acid. The highly π-conjugated system of PANI strongly affected the electrical conductivity of the blend substrate [36]. These ranges of conductivity are sufficient for the conduction of electrical signals in *in vivo* condition [25].

3.2.4 Mechanical properties

According to the mechanical properties of stem cells, the niche can regulate cell behavior such as attachment, migration, and differentiation, so these physical cues have been considered as an essential factor in designing the artificial microenvironment to direct the cell fate [38]. Thus, the scaffold used for nerve tissue engineering must mimic the mechanical properties of the ECM to promote the neural differentiation of stem cells [39]. The elastic modulus (Young's modulus) of substrates at different blend compositions are shown in **Figure 4(b)**. The pure chitosan substrates have lower Young's modulus. Addition PANI to CS increases substrate stiffness.

3.2.5 Contact angle

The hydrophilicity of the substrate is an important characteristic that affects cell attachment. Hence, the surface wettability of the flat and cell-imprinted substrates was measured by water contact angle after treatment with NaOH solution **(Figure 5(a))**. Before neutralization, the hydrophilic nature of CS-PANI blends causes the water droplet to absorb too rapidly for the contact angle to be measured. The contact angle increases between 40^{0}-60^{0} by adding PANI to the substrates. Also, the cell-imprinted CS and CS-PANI substrates were slightly more hydrophobic compared to flat CS and CS-PANI, respectively.

3.2.6 Degradation assay

Throughout in vivo tissue regeneration, the substrate should provide the support structure for cell attachment, proliferation, and differentiation. Successful regeneration for peripheral nerve

damage takes 5-8 weeks [40]. Since one of our aims was to evaluate if surface topography might alter the effect of a CS-PANI blend on neural differentiation due to altered biodegradation, the in vitro degradation of substrates in PBS solution was examined for 5 weeks. **Figure 5(b)** shows that the degradation rate of pure CS substrates was faster than other groups, but still preserved approximately 60% of its initial mass over 2 weeks. The conductive substrates displayed slower degradation rates. For instance, these substrates lost approximately 30% of their mass after 2 weeks of incubation. This result indicates that the substrate used here possess sufficient stability for long-term culture, which may be beneficial for inducing cell growth and differentiation.

3.3 Characterization of rat adipose-derived stem cells (rADSCs)

Fibroblast-like and specific CD markers on the cell surface are the most important criteria for the characterization of ADSCs [41-42]. These cells are positive for mesenchymal specific markers such as CD29 and CD90 and negative for hematopoietic stem cell markers such as CD34 and CD45 [43]. The morphology of ADSCs after 5 and 14 days after isolation is shown in **Figure 6(a)**. These cells displayed the adherent and typical fibroblast-like morphology under optical microscopy. Flow cytometry results demonstrated that 99.4% and 98.85% of the cell population were positive for CD90 and CD29, while only 0.122% and 0.457% of them were positive for CD34 and CD45, respectively **(Figure 6(b))**. Immunostaining by CD surface markers was also performed (**Figure 6 (c-f))**. These results revealed that more than 85% of rADSCs positively expressed the mesenchymal stem cell markers CD29 and CD90 but did not express the hematopoietic stem cell marker CD45 and CD34 (< 5%).

3.4 Cell attachment and morphology on substrates.

An optimal biomimetic scaffold should act as a supporting microenvironment for cell attachment, growth, and migration [44-45]. It can be seen in **Figure 7 (a-d)** that the actin cytoskeleton of ADSCs cultured on flat and imprinted substrates. The spindle morphology of cells on flat substrates and bipolar shape of cells on imprinted substrates are visible in these figures.

Figures 7 (e-h) display the morphology of rADSCs grown on the scaffolds as visualized by AFM. The cells were spindle-shaped on flat substrates with effective attachment to these surfaces. In contrast, the ADSCs became more spread and more adhesive on flat CS- PANI

substrate compared to flat pure CS substrates. The fibroblast like shape of ADSCs converted into the elongated and bipolar shape of differentiated PC12 cells, which is represented in **Figure 7 (f).** Therefore, these results demonstrate the adaptation of cells to the specific shapes of the substrate profile. The cells were stretched and tightly attached over conductive substrates. The morphology of the cells on all substrates confirmed excellent cell adhesion property for rADSCs.

3.5 Cell viability study (MTT assay)

The biocompatibility of pure CS substrates and CS-PANI substrates was evaluated by MTT assay to define the effect of the PANI concentration on rADSCs proliferation on 1, 3,7,14 days after cells seeding. The results from the determination of proliferation rate **(Figure 8)** showed no significant difference between cells cultured on typical TCP and cells cultivated on pure CS substrates or CS-PANI substrates. These results confirm the biocompatibility and supporting role of flat and cell-imprinted CS-PANI substrates for adhesion and growth of ADSCs.

3.6 Immunocytochemistry

The effect of cell- imprinting topography and conductivity of the scaffolds on neural differentiation of ADSCs was examined by staining them with MAP2 and GFAP specific antibodies and viewed by fluorescent microscopy (**Figure 9**). MAP2 and GFAP markers are expressed in neuronal cells and astrocyte cells, respectively. The results of the immunocytochemistry supported western blot analysis. After 8 days, more ADSCs on imprinted substrates were more immunoreactive for GFAP and MAP2 markers relative to ADSCs that, were cultured on flat substrates, suggesting significant the topography-driven neural differentiation. Furthermore, by adding PANI to the substrate, the level of expression of neural-specific genes and, consequently, the degree of differentiation was enhanced. Hence, the CI (CS-PANI) groups were found to have the highest level of expression for both markers among the experimental groups.

4. Discussion

Several studies emphasize that the physical characteristics of synthetic surfaces such as topographic features at the micro- and nanoscale [46] and conductivity [47]can regulate the behavior

of the mammalian cells [48-49]. Micro- and nanoscale topography can direct cell fate through the activation of mechanotransduction pathways, rearranging the alignment of the cytoskeleton and nuclear shape and ultimately altering transcription programs and protein expression [50-52].

Also, endogenous electric fields in tissues such as nerve, heart, and bone dictate stem cell differentiation toward a specific lineage of native tissue by alterating membrane depolarization [53-55]. Therefore, recent studies investigate the synergetic effect of these two factors on guiding the differentiation of stem cells into specific cell lineage. Tian et al. fabricated random and aligned conductive nanofibers composed of poly (lactic acid) (PLA) and Ppy by electrospinning to increase the differentiation of PC12 cells. The immunostaining of the neuronal specific proteins, neurofilament 200 (NF200), and alpha tubulin indicated that the neuronal differentiation of PC12 cells on aligned nanofibers was increased by electrical stimulation with a voltage of 40 mV [48]. Therefore, it is imperative to manufacture a biocompatible scaffold with appropriate physical properties such as desirable topography and electrical conductivity to regulate stem cell behavior.

McBeath et al. showed that cell shape has a strong effect on the differentiation of human mesenchymal stem cells (hMSCs) to adipocyte or osteoblast fates [56]. Subsequently, several reports have confirmed that cell shape influences its behavior by applying micro-contact and micro-well printing methods [57-58]. In recent studies, the direct cell-imprinting method has been utilized to promote the differentiation of stem cells by applying cell-like topographies (cell-imprinted substrate) and geometry [46, 59].

Bonakdar et al. demonstrated that the shape, as well as nano and microfeatures of cells' replicated on a PDMS substrate, can regulate stem cell differentiation into the original phenotype of the cells used to mold the substrate. According to these reports, chondrocyte-imprinted substrates provide micro to nanoscale topographical to induce the chondrocyte phenotype into adipose-derived stem cells [22]. Similarly, Machinchian et al. have successfully employed an imprinted substrate based on mature human keratinocyte shape for skin tissue engineering [60]. In most previous studies, silicone (*i.e.*, PDMS) was the shaping material due to its transparency, capability of molding nano/micro-structures, and rubber-like elastic properties. Application of PDMS as a tissue engineering scaffold has several limitations, including non-biodegradability, poor electrical properties, complicated processes for improvement of electrical conducting of this polymer, and undesirable mechanical properties [61-62].

In the current study, we fabricated conductive patterned scaffolds based on CS- PANI hydrogels using a cell- imprinting method to direct the neural differentiation of ADSCs. For this purpose, we blended CS with PANI to develop a conductive hydrogel with appropriate stability, biocompatibility, conductivity, and proper mechanical properties. The blended polymers were poured on fixed PC12 cells and kept at 37 °C for 48 h. The absorption peaks at 3290, 1554, 1519, 1161, 913, and 848 cm^{-1} confirmed PANI's presence in the hydrogels **(Figure 2)**. While no noticeable difference is observed in the obtained flat CS substrate and CS-PANI one (Figure 3a and 3b), bipolar or tripolar spindle morphology of PC12 cells is clearly displayed in SEM images of the imprinted substrate (**Figure 3 (e-f)).** Bonakdar and coworkers used SEM images to show the difference between the morphology of chondrocytes, tenocytes, and ADSCs patterns on imprinted PDMS substrates [22, 63]. In addition, 3D AFM imaging (**Figure 3**(**g**)) and AFM height profiles of a PC12 cell imprinted substrate (**Figure 3**(**h**)) were employed to demonstrate the successful imprinting of the topographical features of PC12 cells.

Since *in vivo* neural communication at synapses occurs through an electrical event (the action potential), electrically conductive scaffolds have great potential in neural tissue engineering [64-65]. The electrical component of the stem cell niche enhances neurotrophin secretion, stem cells' myelin gene expression, and thereby nerve regeneration [66]. The pure chitosan substrates have weak conductivity 7.5×10^{-8} S/cm because of the polarity of protonation of the amino group. We obtained similar results for both flat and imprinted CS substrates (**Figure 4(a)**). Hence, in the present study, we use a conductive polymer such as PANI for blending with CS to enhance the electrical conductivity of the flat and patterned substrates. The results show 4 orders of the magnitude increase in specific conductivity (**Figure 4(a)**), and there was no meaningful difference between the flat and imprinted substrates. The antioxidant properties of the PANI can also scavenge free radicals at the injured site and minimize scar formation, which is a significant barrier to nerve regeneration [36].

Unlike conductivity, cell-imprinting decreases the Young's modulus by 5 % even for pure CS substrate (**Figure 4(b)**). Similar behavior was observed in CS-PANI substrates comparing flat to imprinted substrate. Our conclusion is that imprinting on a flat substrate might create local porosity and thinning of the film in the imprinted parts. The addition of PANI increases the Young's modulus of chitosan blend substrates up to almost 20 % (**Figure 4(b)**). The increased stiffness likely resulted from important effect of PANI in the blend substrate. The brittle and stiff

nature of PANI (Young modulus of PANI is 1.3 GPa) [67] has a tightening effect on blends and improves the mechanical properties of the substrate. The stiffness of all of our samples is suitable for neural differentiation [68].

As indicated earlier, the measured contact angle demonstrates that the hydrophobicity of all substrates is suitable for cell attachment. Therefore, a mechanism distinct from surface chemistry such as substrate stiffness and electrical conductivity directed cell spreading. The result of many investigations has suggested that a high conductivity scaffold enhances the electrostatic interactions between the cell and substrate, leading to improved cell adhesion [69]. The inherent hydrophobic nature of PANI decreases the affinity between the water droplet and the blend substrate, and the uniform incorporation of PANI in the CS substrate leads to a monotonic increase in contact angle (**Figure 5(a)**). Also, Yang et al indicated that the geometrical micro- or nanostructure of the surface increase the hydrophobicity of solid surface[70]. In this study, cell-imprinted substrates were more hydrophobic property than flat substrates. All of the substrates we studied have moderately hydrophilic surfaces with contact angles between 40° and 70°, which are considered appropriate for cell attachment.

The hydrophobic domain of PANI in the CS matrix decreased the hydrophilicity of the substrate and acted as a barrier against water penetration. Thus, the conductive substrates possess a lower degradation rate than a pure CS substrate. Also, cell-imprinted substrates were more hydrophobic relative to flat substrates, and these patterned substrates degraded at a lower rate (**Figure 5(b)**).

Before using of prepared substrates for neural differentiation of ADSCs, The results of flow cytometry and immunocytochemistry confirmed these isolated cells express specific mesenchymal stem cell markers (**Figure 6)**.

The F-actin staining image of ADCSs cultivated on PC12-imprinted substrates (**Figure 7**(**a-d**)) confirms the change in morphology of these cells when they are grown on the patterned substrates. When ADSCs with semi-fibroblast (irregular-spindle) morphology are cultured on PC12- imprinted substrates obtained from bipolar morphology, these cells move into a pattern that can lead to irregular morphology to bipolar spindle morphology, thus further demonstrating the effect of patterned structure on cytoskeleton arrangement (**Figure 7(e-f)**). In a previous study, a nanopatterned substrate induced the cellular reorientation and actin alignment along microgrooves and elevated focal adhesion formation and cytoskeletal reorganization. These mechanisms lead to activation of integrin-mediated mechanotransduction and intracellular

signaling pathways such as β1-integrin binding/clustering and myosin-actin interaction, and the Rho-associated protein kinase (ROCK) and mitogen-activated protein kinase/extracellular signal regulated kinase (MEK-ERK) pathways. These signaling pathways accelerated the differentiation of hNSCs into dopaminergic and glutamatergic neurons with electrophysiological properties [47]. What this study adds to the analysis of shape on cell function is the fact that creating a gradual increase and decrease in height and depth that mimics the cellular environment has a greater effect on the mechanotransduction leading to neural cells phonotype than that of any other cell-type that have been studied (Figure 7 d compared to 7b and the ratio comparison in Figure 7j). This improvement happens despite the imprinted substrate having lower Young's modulus than the flat one (Figure 4b), which shows the topographic characteristic has taken over the stiffness of the substrate. Also, we showed the PANI did not have a toxic effect on the biocompatibility of CS with these cell cultures (**Figure 8**). This results is important, considering that conductive polymers such as PANI must be used in optimal concentration to be compatible for cells [71].

A similar effect can be concluded from our results of immunocytochemistry staining (**Figures 9**), which confirmed an enhanced neural differentiation in the stem cells cultured on the PC12-imprinted substrate compared to those cultured on the flat substrate. MAP2 isoforms are expressed only in neuronal cells, while GFAP is expressed in astrocyte cells and contributes to many important CNS processes, including cell communication and the functioning of the blood brain barrier [72]. Here, the CI (CS-PANI) displayed the highest potential for neuron and astrocyte differentiation, according to the up-regulation of MAP2 and GFAP. Moreover, this study verified that PANI, as a conductive polymer, provided a pathway to guide ADSC differentiation towards neuronal lineages without any adverse effect on cell biocompatibility. The higher expression of MAP2 and GFAP on conductive substrate relative to non-conductive substrates supports the importance of electrical signaling for neuronal differentiation. This feature of PC12-imprinting along with their topographic effect on ADSCs elongation, proliferation, and differentiation suggest that these engineered substrates are suitable for increased neuronal differentiation.

5. Conclusion

The substrates produced for neurogenic differentiation effectively simulate the natural ECM of neuron cells in multiple aspects. In this study, conductive cell-imprinted substrates mimic the

topography and conductivity of nerve tissue, which can physically direct stem cells toward neuron like cells. PC12-imprinted CS-PANI substrates exhibit desirable characteristics such as appropriate mechanical properties, degradation rate, and good wettability, which represent effective parameters stimulating neural differentiation. Finally, this work prepares a pioneered design of patterned conductive scaffolds for controlling the differentiation of ADSCs, which has the potential for effective stem cell therapy of neurological diseases and injury. This synergetic effects and the comparison between the mechanical strength, topography, and electro-conductivity propose that by trying to bring more cues to the neural tissue engineering, mechanotransduction can be used as one of the main reasons for nonconventional results but at the main time push us toward thermodynamic parameters of the cell structure.

- **Conflicts of interest**

There are no conflicts of interest to declare.

- **Acknowledgements**

The authors would like to thank support from Amirkabir University and Technology, NSF DMR-1720530 and CMMI-154857 US National Science Foundation.

- **References**

(1) Beynon, V.; Raheja, R.; Mazzola, M.; Weiner, H. The Central and Peripheral Nervous System Immunological Compartments in Health and Disease. In *Neurorheumatology*; Springer: 2019; pp 3-9.
(2) Horner, P. J.; Gage, F. H. Regenerating the damaged central nervous system. *Nature* **2000,** *407* (6807), 963-970.
(3) Rocca, W. A.; Petersen, R. C.; Knopman, D. S.; Hebert, L. E.; Evans, D. A.; Hall, K. S.; Gao, S.; Unverzagt, F. W.; Langa, K. M.; Larson, E. B. Trends in the incidence and prevalence of Alzheimer's disease, dementia, and cognitive impairment in the United States. *Alzheimer's & Dementia* **2011,** *7* (1), 80-93.
(4) Ketchum, J. M.; Cuthbert, J. P.; Deutsch, A.; Chen, Y.; Charlifue, S.; Chen, D.; Dijkers, M. P.; Graham, J. E.; Heinemann, A. W.; Lammertse, D. P. Representativeness of the Spinal Cord Injury Model Systems National Database. *Spinal cord* **2018,** *56* (2), 126-132.
(5) Jessen, K.; Mirsky, R. The repair Schwann cell and its function in regenerating nerves. *The Journal of physiology* **2016,** *594* (13), 3521-3531.
(6) Hermanns, S.; Klapka, N.; Gasis, M.; Müller, H. W. The collagenous wound healing scar in the injured central nervous system inhibits axonal regeneration. In *Brain Repair*; Springer: 2006; pp 177-190.
(7) Wu, Y.; Wang, L.; Guo, B.; Shao, Y.; Ma, P. X. Electroactive biodegradable polyurethane significantly enhanced Schwann cells myelin gene expression and neurotrophin secretion for peripheral nerve tissue engineering. *Biomaterials* **2016,** *87*, 18-31.

(8) Lindvall, O.; Kokaia, Z. Stem cells for the treatment of neurological disorders. *Nature* **2006,** *441* (7097), 1094-1096.
(9) Hasan, A.; Deeb, G.; Rahal, R.; Atwi, K.; Mondello, S.; Marei, H. E.; Gali, A.; Sleiman, E. Mesenchymal stem cells in the treatment of traumatic brain injury. *Frontiers in neurology* **2017,** *8*, 28.
(10) Park, J.; Kim, P.; Helen, W.; Engler, A. J.; Levchenko, A.; Kim, D.-H. Control of stem cell fate and function by engineering physical microenvironments. *Integrative biology* **2012,** *4* (9), 1008-1018.
(11) Rando, T. A.; Ambrosio, F. Regenerative rehabilitation: applied biophysics meets stem cell therapeutics. *Cell Stem Cell* **2018,** *22* (3), 306-309.
(12) Janmey, P. A.; Fletcher, D.; Reinhart-King, C. A. Stiffness Sensing in Cells and Tissues. *Physiological reviews* **2019**.
(13) Liu, W. F.; Chen, C. S. Engineering biomaterials to control cell function. *Materials Today* **2005,** *8* (12), 28-35.
(14) Georgiou, M.; Golding, J. P.; Loughlin, A. J.; Kingham, P. J.; Phillips, J. B. Engineered neural tissue with aligned, differentiated adipose-derived stem cells promotes peripheral nerve regeneration across a critical sized defect in rat sciatic nerve. *Biomaterials* **2015,** *37*, 242-251.
(15) Onesto, V.; Cancedda, L.; Coluccio, M.; Nanni, M.; Pesce, M.; Malara, N.; Cesarelli, M.; Di Fabrizio, E.; Amato, F.; Gentile, F. Nano-topography enhances communication in neural cells networks. *Scientific reports* **2017,** *7* (1), 1-13.
(16) Zhang, Y.; Gordon, A.; Qian, W.; Chen, W. Engineering nanoscale stem cell niche: direct stem cell behavior at cell–matrix interface. *Advanced healthcare materials* **2015,** *4* (13), 1900-1914.
(17) Ermis, M.; Antmen, E.; Hasirci, V. Micro and Nanofabrication methods to control cell-substrate interactions and cell behavior: A review from the tissue engineering perspective. *Bioactive materials* **2018,** *3* (3), 355-369.
(18) Ventre, M.; Netti, P. A. Engineering cell instructive materials to control cell fate and functions through material cues and surface patterning. *ACS applied materials & interfaces* **2016,** *8* (24), 14896-14908.
(19) Heydari, T.; Heidari, M.; Mashinchian, O.; Wojcik, M.; Xu, K.; Dalby, M. J.; Mahmoudi, M.; Ejtehadi, M. R. Development of a virtual cell model to predict cell response to substrate topography. *ACS nano* **2017,** *11* (9), 9084-9092.
(20) Jain, D.; Mattiassi, S.; Goh, E. L.; Yim, E. K. Extracellular matrix and biomimetic engineering microenvironment for neuronal differentiation. *Neural regeneration research* **2020,** *15* (4), 573.
(21) Mahmoudi, M.; Bonakdar, S.; Shokrgozar, M. A.; Aghaverdi, H.; Hartmann, R.; Pick, A.; Witte, G.; Parak, W. J. Cell-imprinted substrates direct the fate of stem cells. *ACS nano* **2013,** *7* (10), 8379-8384.
(22) Bonakdar, S.; Mahmoudi, M.; Montazeri, L.; Taghipoor, M.; Bertsch, A.; Shokrgozar, M. A.; Sharifi, S.; Majidi, M.; Mashinchian, O.; Hamrang Sekachaei, M. Cell-imprinted substrates modulate differentiation, redifferentiation, and transdifferentiation. *ACS applied materials & interfaces* **2016,** *8* (22), 13777-13784.
(23) Moosazadeh Moghaddam, M.; Bonakdar, S.; Shokrgozar, M. A.; Zaminy, A.; Vali, H.; Faghihi, S. Engineered substrates with imprinted cell-like topographies induce direct differentiation of adipose-derived mesenchymal stem cells into Schwann cells. *Artificial cells, nanomedicine, and biotechnology* **2019,** *47* (1), 1022-1035.
(24) Zhu, W.; Ye, T.; Lee, S.-J.; Cui, H.; Miao, S.; Zhou, X.; Shuai, D.; Zhang, L. G. Enhanced neural stem cell functions in conductive annealed carbon nanofibrous scaffolds with electrical stimulation. *Nanomedicine: Nanotechnology, Biology and Medicine* **2018,** *14* (7), 2485-2494.
(25) Zhu, R.; Sun, Z.; Li, C.; Ramakrishna, S.; Chiu, K.; He, L. Electrical stimulation affects neural stem cell fate and function in vitro. *Experimental Neurology* **2019,** *319*, 112963.

(26) Guo, B.; Ma, P. X. Conducting polymers for tissue engineering. *Biomacromolecules* **2018,** *19* (6), 1764-1782.
(27) Ahsan, S. M.; Thomas, M.; Reddy, K. K.; Sooraparaju, S. G.; Asthana, A.; Bhatnagar, I. Chitosan as biomaterial in drug delivery and tissue engineering. *International journal of biological macromolecules* **2018,** *110*, 97-109.
(28) Rodríguez-Vázquez, M.; Vega-Ruiz, B.; Ramos-Zúñiga, R.; Saldaña-Koppel, D. A.; Quiñones-Olvera, L. F. Chitosan and its potential use as a scaffold for tissue engineering in regenerative medicine. *BioMed research international* **2015,** *2015*.
(29) Farhadihosseinabadi, B.; Zarebkohan, A.; Eftekhary, M.; Heiat, M.; Moghaddam, M. M.; Gholipourmalekabadi, M. Crosstalk between chitosan and cell signaling pathways. *Cellular and Molecular Life Sciences* **2019**, 1-22.
(30) Zhao, X.; Li, P.; Guo, B.; Ma, P. X. Antibacterial and conductive injectable hydrogels based on quaternized chitosan-graft-polyaniline/oxidized dextran for tissue engineering. *Acta biomaterialia* **2015,** *26*, 236-248.
(31) Orlowska, A.; Perera, P. T.; Al Kobaisi, M.; Dias, A.; Nguyen, H. K. D.; Ghanaati, S.; Baulin, V.; Crawford, R. J.; Ivanova, E. P. The effect of coatings and nerve growth factor on attachment and differentiation of pheochromocytoma cells. *Materials* **2018,** *11* (1), 60.
(32) Baniasadi, H.; SA, A. R.; Mashayekhan, S. Fabrication and characterization of conductive chitosan/gelatin-based scaffolds for nerve tissue engineering. *International journal of biological macromolecules* **2015,** *74*, 360-366.
(33) Sun, J.; Liu, W. H.; Deng, F. M.; Luo, Y. H.; Wen, K.; Zhang, H.; Liu, H. R.; Wu, J.; Su, B. Y.; Liu, Y. L. Differentiation of rat adipose derived mesenchymal stem cells into corneal like epithelial cells driven by PAX6. *Experimental and therapeutic medicine* **2018,** *15* (2), 1424-1432.
(34) Nunthanid, J.; Laungtana-Anan, M.; Sriamornsak, P.; Limmatvapirat, S.; Puttipipatkhachorn, S.; Lim, L. Y.; Khor, E. Characterization of chitosan acetate as a binder for sustained release tablets. *Journal of Controlled Release* **2004,** *99* (1), 15-26.
(35) Osman, Z.; Arof, A. K. FTIR studies of chitosan acetate based polymer electrolytes. *Electrochimica Acta* **2003,** *48* (8), 993-999.
(36) Gizdavic-Nikolaidis, M. R.; Stanisavljev, D. R.; Easteal, A. J.; Zujovic, Z. D. Microwave-assisted synthesis of functionalized polyaniline nanostructures with advanced antioxidant properties. *The Journal of Physical Chemistry C* **2010,** *114* (44), 18790-18796.
(37) Yavuz, A. G.; Uygun, A.; Bhethanabotla, V. R. Preparation of substituted polyaniline/chitosan composites by in situ electropolymerization and their application to glucose sensing. *Carbohydrate Polymers* **2010,** *81* (3), 712-719.
(38) Discher, D. E.; Janmey, P.; Wang, Y.-l. Tissue cells feel and respond to the stiffness of their substrate. *Science* **2005,** *310* (5751), 1139-1143.
(39) Seidlits, S. K.; Khaing, Z. Z.; Petersen, R. R.; Nickels, J. D.; Vanscoy, J. E.; Shear, J. B.; Schmidt, C. E. The effects of hyaluronic acid hydrogels with tunable mechanical properties on neural progenitor cell differentiation. *Biomaterials* **2010,** *31* (14), 3930-3940.
(40) Guilak, F.; Cohen, D. M.; Estes, B. T.; Gimble, J. M.; Liedtke, W.; Chen, C. S. Control of stem cell fate by physical interactions with the extracellular matrix. *Cell stem cell* **2009,** *5* (1), 17-26.
(41) Jiang, L.; Zhu, J.-K.; Liu, X.-L.; Xiang, P.; Hu, J.; Yu, W.-H. Differentiation of rat adipose tissue-derived stem cells into Schwann-like cells in vitro. *Neuroreport* **2008,** *19* (10), 1015-1019.
(42) Lopez, M. J.; Spencer, N. D. In vitro adult rat adipose tissue-derived stromal cell isolation and differentiation. In *Adipose-Derived Stem Cells*; Springer: 2011; pp 37-46.

(43) Sgodda, M.; Aurich, H.; Kleist, S.; Aurich, I.; König, S.; Dollinger, M. M.; Fleig, W. E.; Christ, B. Hepatocyte differentiation of mesenchymal stem cells from rat peritoneal adipose tissue in vitro and in vivo. *Experimental cell research* **2007,** *313* (13), 2875-2886.
(44) Negah, S. S.; Khaksar, Z.; Aligholi, H.; Sadeghi, S. M.; Mousavi, S. M. M.; Kazemi, H.; Jahan-Abad, A. J.; Gorji, A. Enhancement of neural stem cell survival, proliferation, migration, and differentiation in a novel self-assembly peptide nanofibber scaffold. *Molecular neurobiology* **2017,** *54* (10), 8050-8062.
(45) Muerza-Cascante, M. L.; Shokoohmand, A.; Khosrotehrani, K.; Haylock, D.; Dalton, P. D.; Hutmacher, D. W.; Loessner, D. Endosteal-like extracellular matrix expression on melt electrospun written scaffolds. *Acta biomaterialia* **2017,** *52*, 145-158.
(46) Abagnale, G.; Sechi, A.; Steger, M.; Zhou, Q.; Kuo, C.-C.; Aydin, G.; Schalla, C.; Müller-Newen, G.; Zenke, M.; Costa, I. G. Surface topography guides morphology and spatial patterning of induced pluripotent stem cell colonies. *Stem cell reports* **2017,** *9* (2), 654-666.
(47) Yang, K.; Yu, S. J.; Lee, J. S.; Lee, H.-R.; Chang, G.-E.; Seo, J.; Lee, T.; Cheong, E.; Im, S. G.; Cho, S.-W. Electroconductive nanoscale topography for enhanced neuronal differentiation and electrophysiological maturation of human neural stem cells. *Nanoscale* **2017,** *9* (47), 18737-18752.
(48) Tian, L.; Prabhakaran, M. P.; Hu, J.; Chen, M.; Besenbacher, F.; Ramakrishna, S. Synergistic effect of topography, surface chemistry and conductivity of the electrospun nanofibrous scaffold on cellular response of PC12 cells. *Colloids and Surfaces B: Biointerfaces* **2016,** *145*, 420-429.
(49) Eftekhari, B. S.; Eskandari, M.; Janmey, P. A.; Samadikuchaksaraei, A.; Gholipourmalekabadi, M. Surface Topography and Electrical Signaling: Single and Synergistic Effects on Neural Differentiation of Stem Cells. *Advanced Functional Materials* **2020**, 1907792.
(50) Metavarayuth, K.; Sitasuwan, P.; Zhao, X.; Lin, Y.; Wang, Q. Influence of surface topographical cues on the differentiation of mesenchymal stem cells in vitro. *ACS Biomaterials Science & Engineering* **2016,** *2* (2), 142-151.
(51) Dalby, M. J.; Gadegaard, N.; Oreffo, R. O. Harnessing nanotopography and integrin–matrix interactions to influence stem cell fate. *Nature materials* **2014,** *13* (6), 558-569.
(52) McNamara, L. E.; McMurray, R. J.; Biggs, M. J.; Kantawong, F.; Oreffo, R. O.; Dalby, M. J. Nanotopographical control of stem cell differentiation. *Journal of tissue engineering* **2010,** *1* (1), 120623.
(53) Sundelacruz, S.; Levin, M.; Kaplan, D. L. Comparison of the depolarization response of human mesenchymal stem cells from different donors. *Scientific reports* **2015,** *5*, 18279.
(54) Lynch, K.; Skalli, O.; Sabri, F. Growing neural PC-12 cell on crosslinked silica aerogels increases neurite extension in the presence of an electric field. *Journal of functional biomaterials* **2018,** *9* (2), 30.
(55) Thrivikraman, G.; Madras, G.; Basu, B. Intermittent electrical stimuli for guidance of human mesenchymal stem cell lineage commitment towards neural-like cells on electroconductive substrates. *Biomaterials* **2014,** *35* (24), 6219-6235.
(56) McBeath, R.; Pirone, D. M.; Nelson, C. M.; Bhadriraju, K.; Chen, C. S. Cell shape, cytoskeletal tension, and RhoA regulate stem cell lineage commitment. *Developmental cell* **2004,** *6* (4), 483-495.
(57) Schiffhauer, E. S.; Robinson, D. N. Mechanochemical signaling directs cell-shape change. *Biophysical journal* **2017,** *112* (2), 207-214.
(58) Nagase, K.; Shukuwa, R.; Onuma, T.; Yamato, M.; Takeda, N.; Okano, T. Micro/nano-imprinted substrates grafted with a thermoresponsive polymer for thermally modulated cell separation. *Journal of Materials Chemistry B* **2017,** *5* (30), 5924-5930.
(59) Kim, B. S.; Lee, J.-S.; Gao, G.; Cho, D.-W. Direct 3D cell-printing of human skin with functional transwell system. *Biofabrication* **2017,** *9* (2), 025034.
(60) Mashinchian, O.; Bonakdar, S.; Taghinejad, H.; Satarifard, V.; Heidari, M.; Majidi, M.; Sharifi, S.; Peirovi, A.; Saffar, S.; Taghinejad, M. Cell-imprinted substrates act as an artificial niche for skin regeneration. *ACS applied materials & interfaces* **2014,** *6* (15), 13280-13292.

(61) Mata, A.; Fleischman, A. J.; Roy, S. Characterization of polydimethylsiloxane (PDMS) properties for biomedical micro/nanosystems. *Biomedical microdevices* **2005,** *7* (4), 281-293.
(62) Niu, X.; Peng, S.; Liu, L.; Wen, W.; Sheng, P. Characterizing and patterning of PDMS-based conducting composites. *Advanced Materials* **2007,** *19* (18), 2682-2686.
(63) Kamguyan, K.; Katbab, A. A.; Mahmoudi, M.; Thormann, E.; Moghaddam, S. Z.; Moradi, L.; Bonakdar, S. An engineered cell-imprinted substrate directs osteogenic differentiation in stem cells. *Biomaterials science* **2018,** *6* (1), 189-199.
(64) Gu, X.; Ding, F.; Williams, D. F. Neural tissue engineering options for peripheral nerve regeneration. *Biomaterials* **2014,** *35* (24), 6143-6156.
(65) Xu, H.; Holzwarth, J. M.; Yan, Y.; Xu, P.; Zheng, H.; Yin, Y.; Li, S.; Ma, P. X. Conductive PPY/PDLLA conduit for peripheral nerve regeneration. *Biomaterials* **2014,** *35* (1), 225-235.
(66) Jin, G.; Li, K. The electrically conductive scaffold as the skeleton of stem cell niche in regenerative medicine. *Materials Science and Engineering: C* **2014,** *45*, 671-681.
(67) Valentová, H.; Stejskal, J. Mechanical properties of polyaniline. *Synthetic Metals* **2010,** *160* (7-8), 832-834.
(68) Palchesko, R. N.; Zhang, L.; Sun, Y.; Feinberg, A. W. Development of polydimethylsiloxane substrates with tunable elastic modulus to study cell mechanobiology in muscle and nerve. *PloS one* **2012,** *7* (12).
(69) Kim, Y. S.; Cho, K.; Lee, H. J.; Chang, S.; Lee, H.; Kim, J. H.; Koh, W.-G. Highly conductive and hydrated PEG-based hydrogels for the potential application of a tissue engineering scaffold. *Reactive and Functional Polymers* **2016,** *109*, 15-22.
(70) Yang, C.; Tartaglino, U.; Persson, B. Influence of surface roughness on superhydrophobicity. *Physical review letters* **2006,** *97* (11), 116103.
(71) Kaur, G.; Adhikari, R.; Cass, P.; Bown, M.; Gunatillake, P. Electrically conductive polymers and composites for biomedical applications. *Rsc Advances* **2015,** *5* (47), 37553-37567.
(72) Mattotti, M.; Alvarez, Z.; Delgado, L.; Mateos-Timoneda, M. A.; Aparicio, C.; Planell, J. A.; Alcántara, S.; Engel, E. Differential neuronal and glial behavior on flat and micro patterned chitosan films. *Colloids and Surfaces B: Biointerfaces* **2017,** *158*, 569-577.

Figure 1

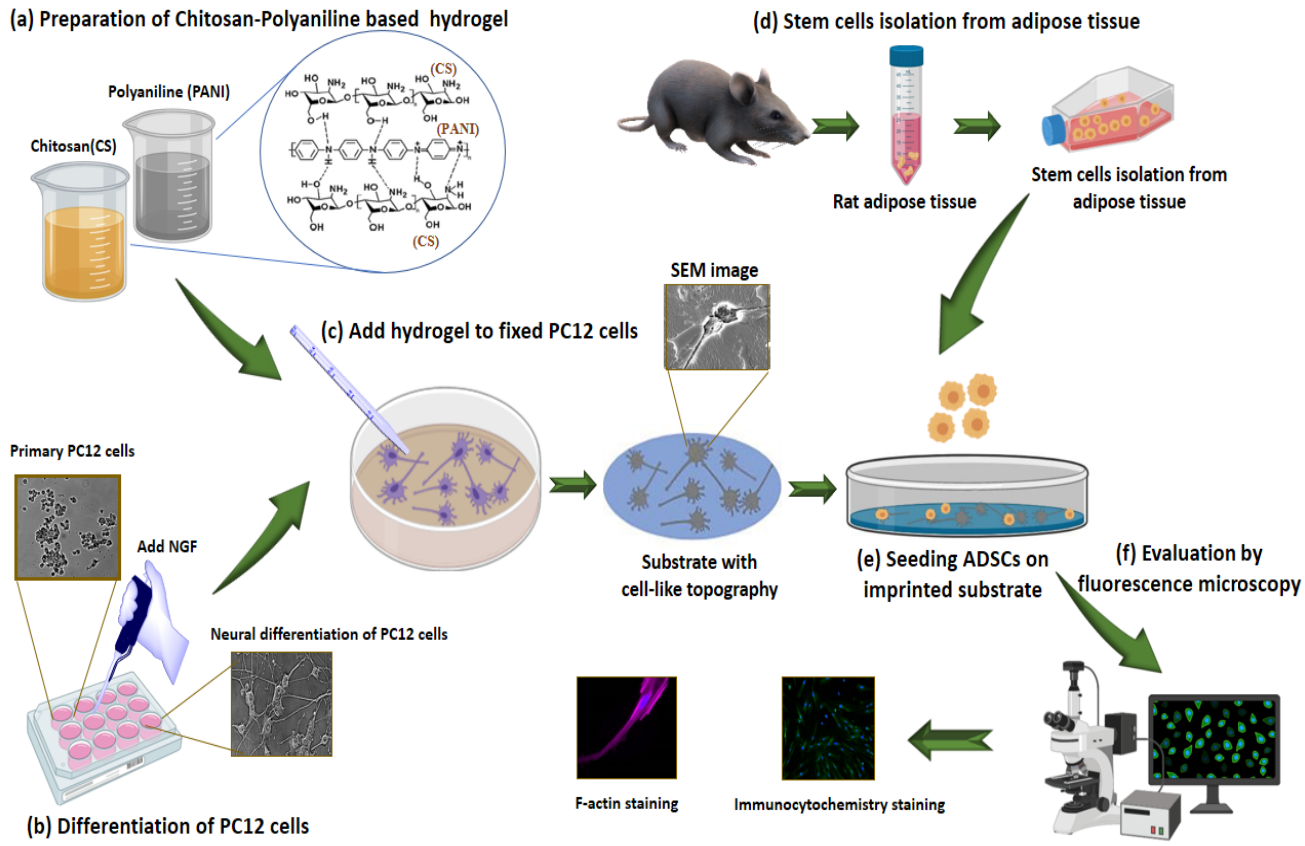

Figure 1: Schematic represents the experiment steps**:** (a) Chitosan- polyaniline based hydrogel was prepared, and (b) PC12 cells were differentiated into neural cells using NGF. (c) After the fixation of these cells, PC12 morphologies were transferred to prepared hydrogel by mold casting. In the next step, (d) stem cells were isolated from rat adipose tissue, and (e) these cells

were cultured on the imprinted substrate. After 8 days, (f) the neural differentiation of rADSCs was evaluated.

Figure 2

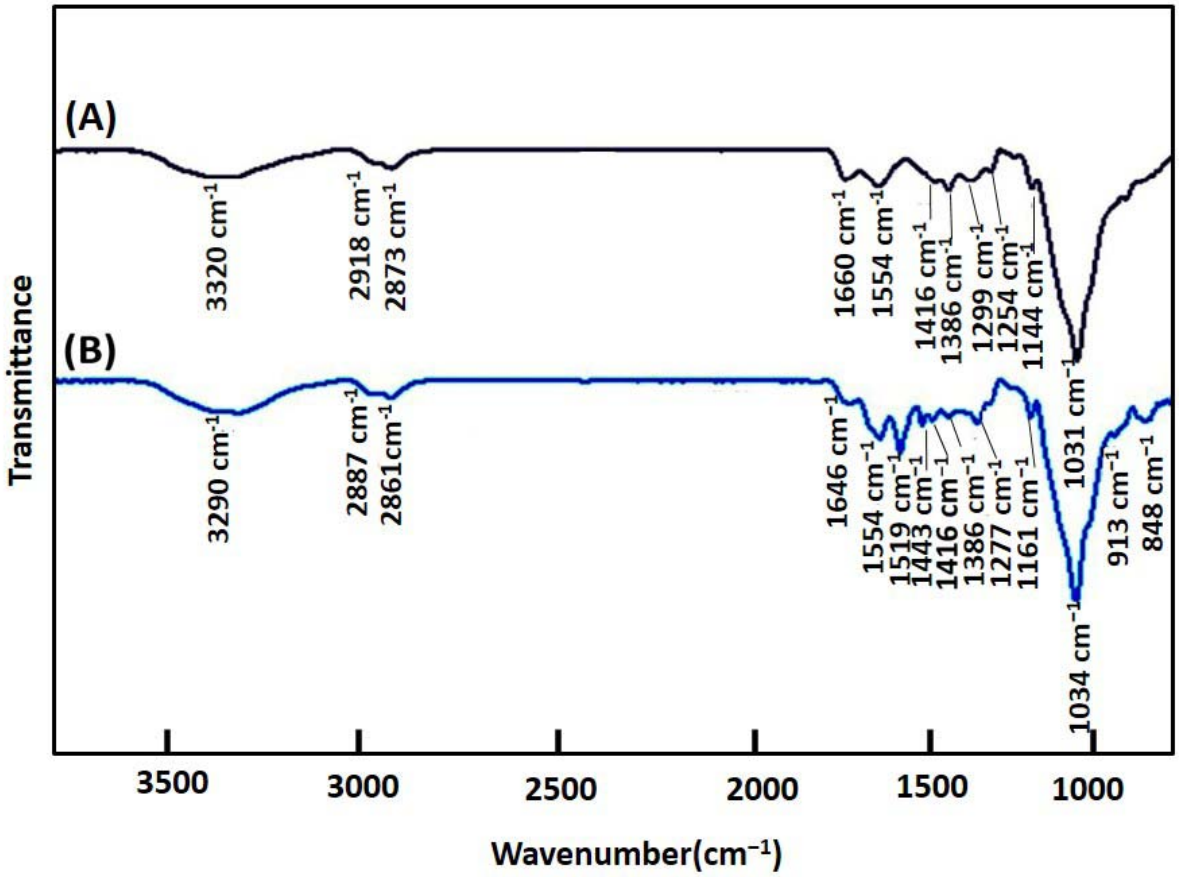

Figure 2: FTIR spectra of A) CS and B) CS-PANI blend substrate are shown. The exhibition of peaks at 1646 cm^{-1}, 1519 cm-^{1}, 1443 cm^{-1}, 1277 cm^{-1} , and 1144 cm^{-1} peaks in the spectra of CS-PANI blend confirm that this substrate includes PANI.

Figure 3

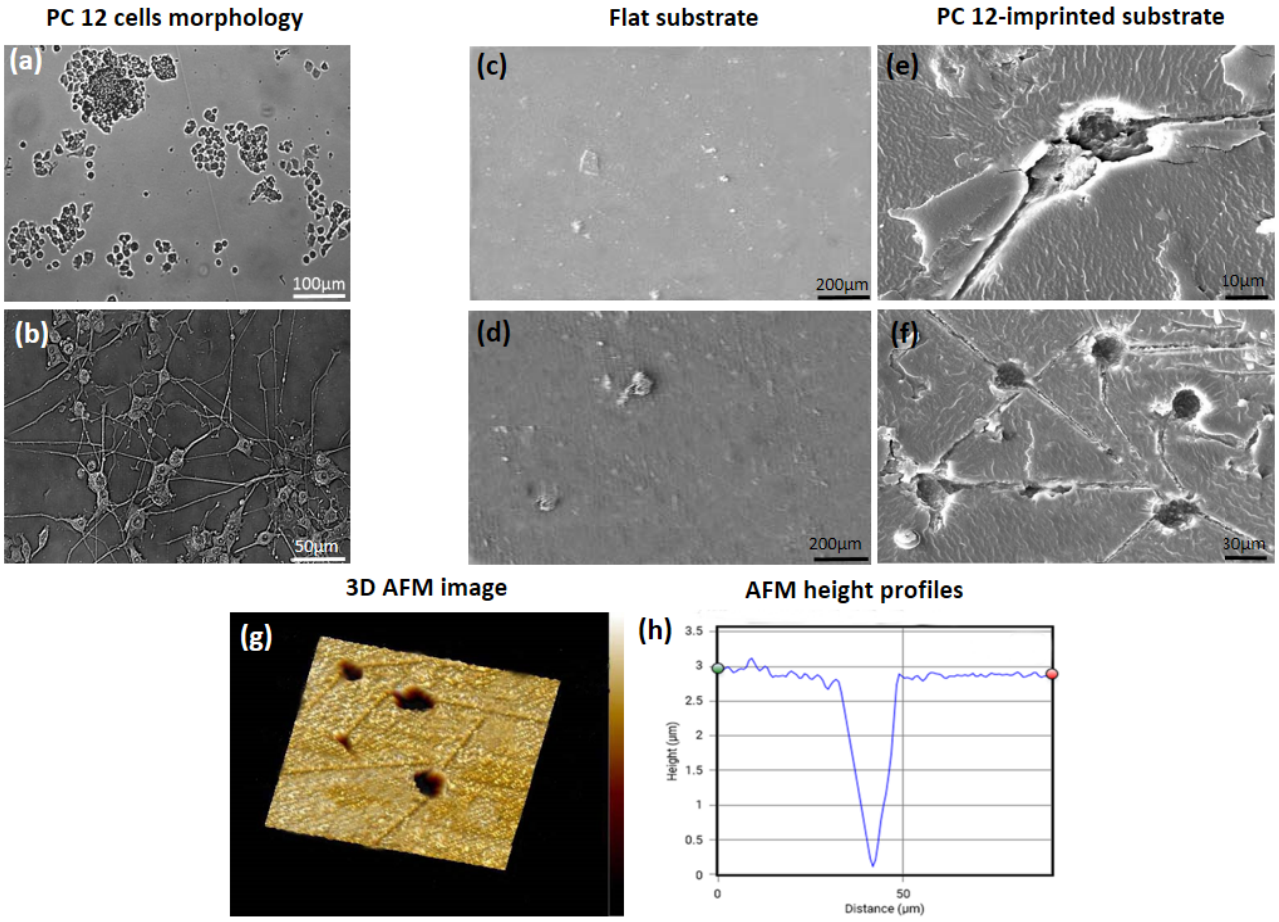

Figure3. (a): Optical image of PC12 cell culture immediately after attachment. (b): Optical image of differentiated PC12 cells. (c): SEM image of flat CS substrate. (d): SEM image of flat

CS-PANI substrate. Topographical features of PC12 cell-imprinted substrates are shown by SEM imaging (e): PC12 cell imprinted CS substrate (f): PC12 cell imprinted CS-PANI substrate, and 3D AFM imaging (g) from a low density of PC12 cells imprinted CS-PANI substrate. (h): AFM height profiles are obtained from one cell representative shape.

Figure 4

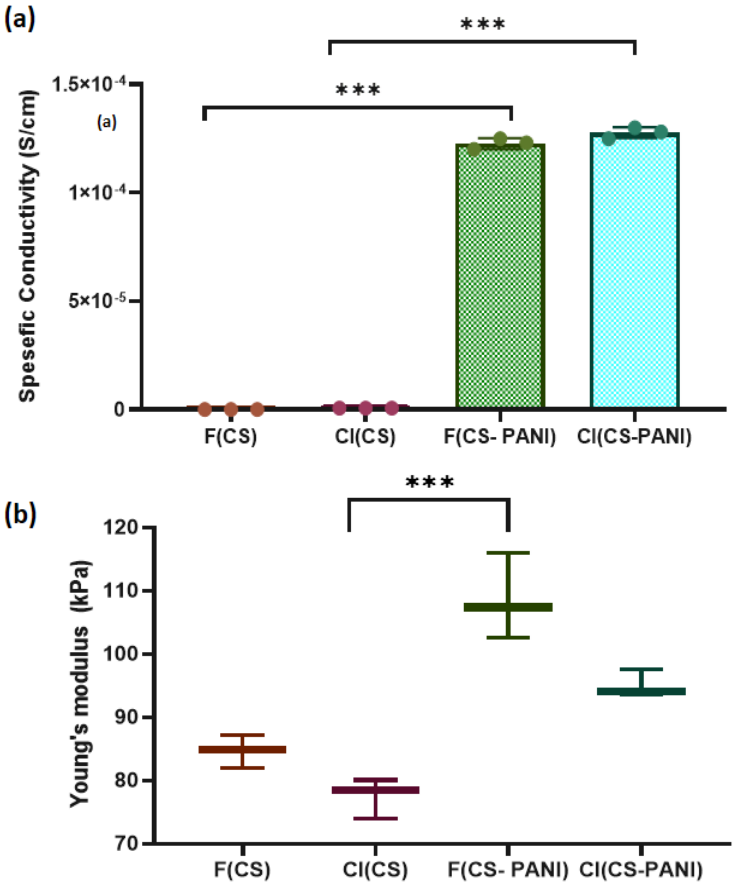

Figure 4. (a): The electrical conductivity of the substrates was increased by adding PANI to pure CS for both flat and cell-imprinted substrates. Flat (F) and cell-imprinted (CI) substrates: F (CS), F (CS-PANI), CI (CS), CI (CS-PANI). Error bars represent the SD of measurements performed

on 4 samples (P < 0.0001). (b): Young's modulus of fabricated flat (F) and cell-imprinted (CI) substrates: F (CS), F (CS-PANI), CI (CS), CI (CS-PANI). (***P <0.05).

Figure 5

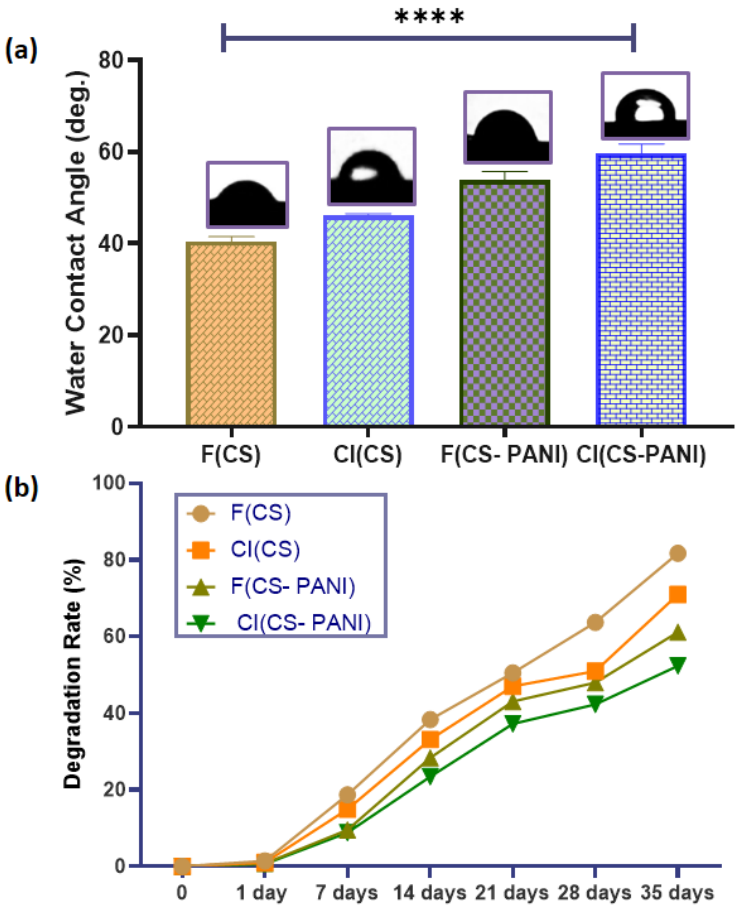

Figure 5. (a): Characterization of wettability of various samples. Water contact angle measurement. (b): *In vitro* biodegradation of prepared substrates in PBS was examined over 5 weeks. ****$P < 0.0001$.

Figure 6

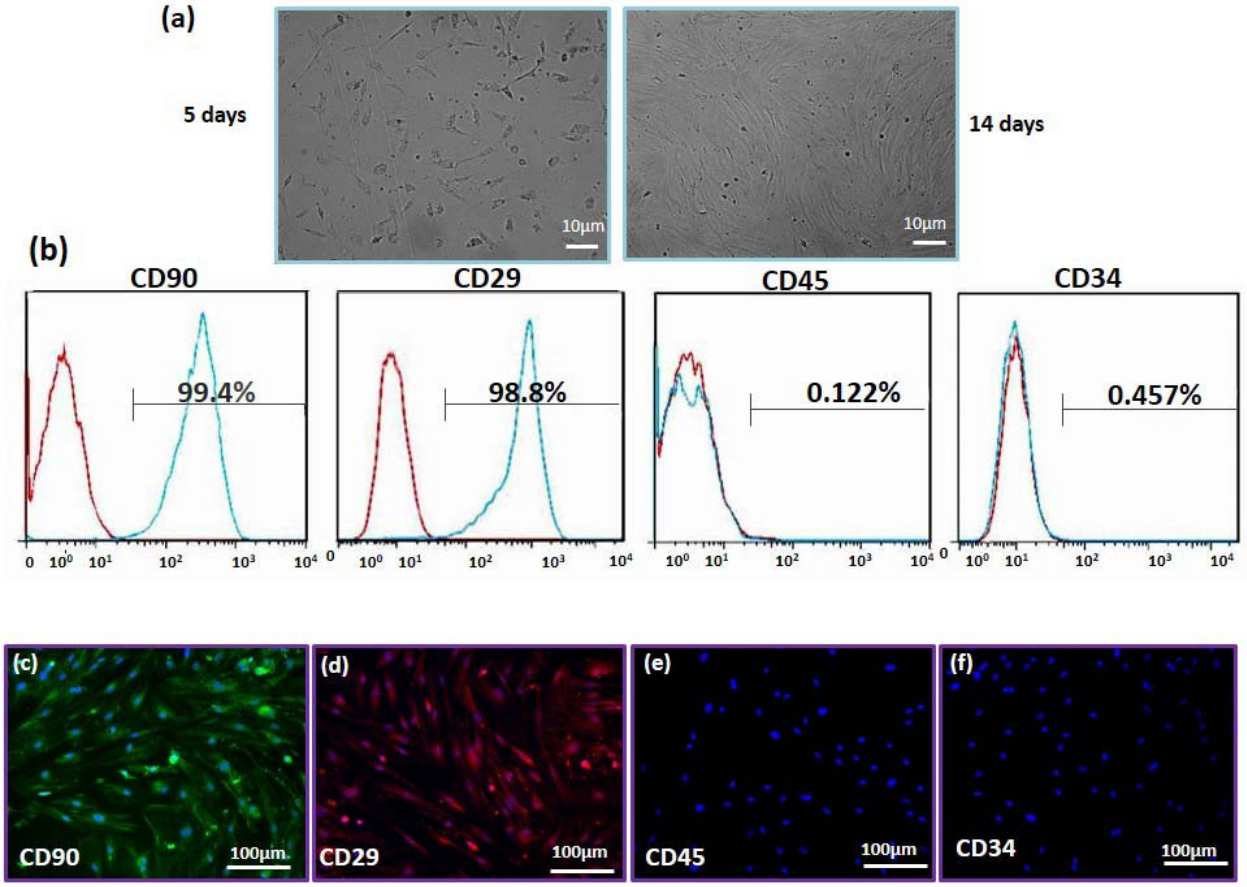

Figure 6. (a): Morphological change in ADSCs in cell culture media at days 5 and 14 post-isolation. (b): Flow cytometry results of CD90, CD29, CD45 and CD34. More than 90% of cell population represented phenotypic characteristics of ADSCs. Immunostaining of the rADSCs expression of (c):CD90 (green), (d): CD29 (red), (e): CD45 and (f): CD34. Cell nuclei were stained with DAPI (blue). The result of staining confirmed the flow cytometry results.

Figure7

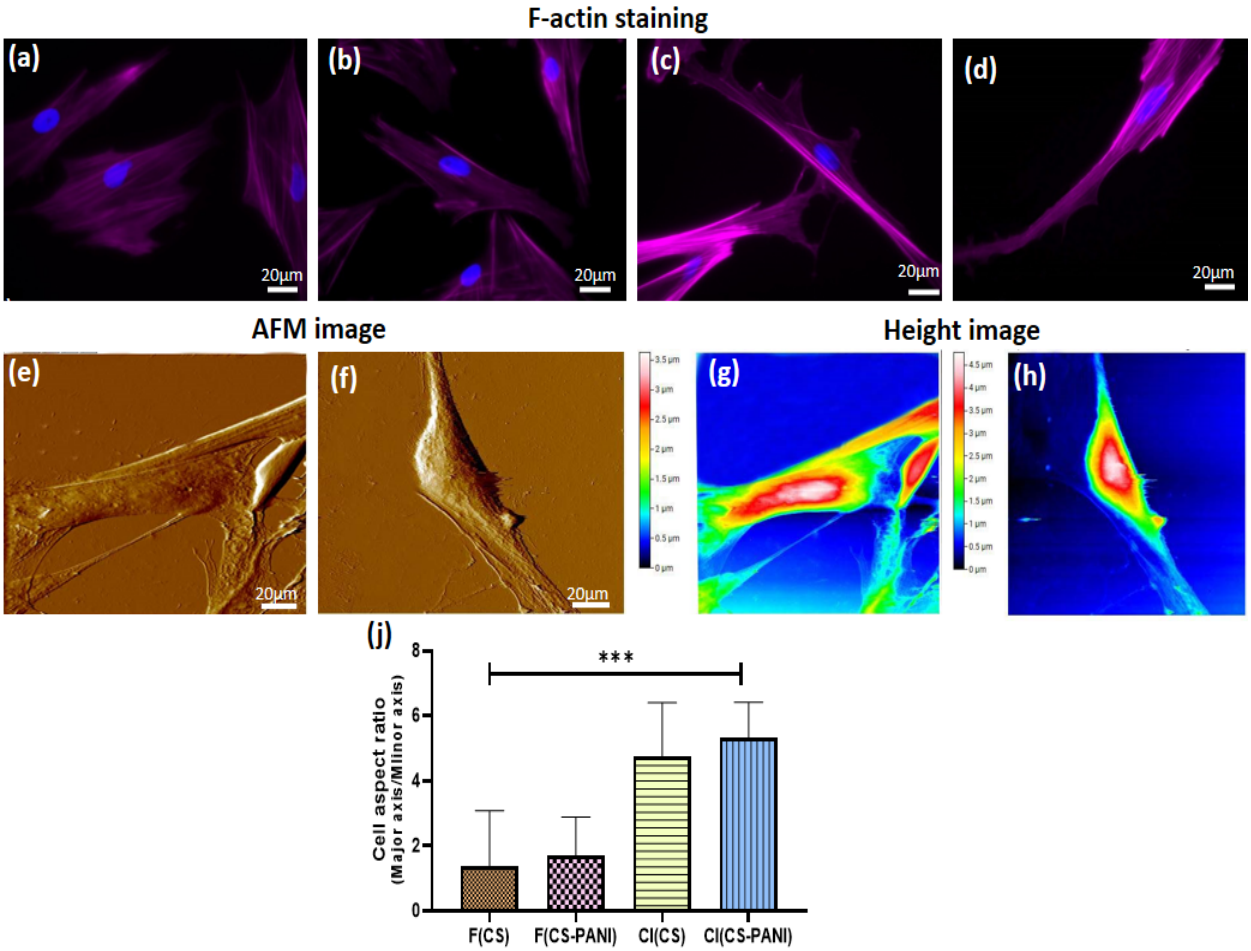

Figure 7: Cell attachment on flat and cell-imprinted substrates. First row: F-actin in rADSCs on flat and cell-imprinted substrates was visualized by phalloidin staining 72 h of seeding. Fluorescence micrographs of rADSCs are representative images for each group. (a): F (CS). (b): F (CS-PANI), (c): CI (CS), (d): CI (CS-PANI). Scale bar: 20µm. Second row: AFM image of rADSCs cultured after 8 days on flat (e) and cell-imprinted (f) substrates. Scale bar: 20µm. Third row: height profile image of cells attached on substrates. (g): Height image of ADSCs on flat substrate. (h): Height image of ADSC on imprinted substrate. (j): Cell morphology aspect ratio of rADSCs on flat CS, flat CS-PANI, patterned pure CS and patterned CS-PANI substrates. (*$p < 0.05$).

Figure 8

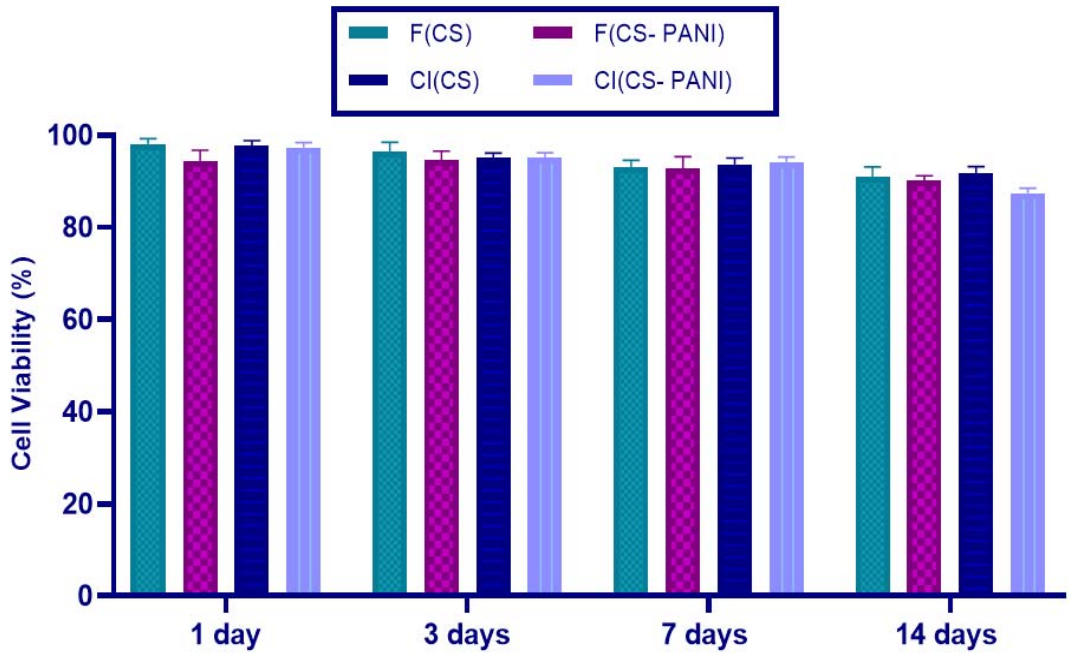

Figure 8: MTT viability assay of cultured ADSCs on the prepared substrates. F (CS): Flat chitosan substrate, F (CS-PANI): Flat chitosan-polyaniline substrate, CI (CS): cell-imprinted chitosan substrate, CI (CS-PANI): cell-imprinted chitosan- polyaniline substrate. (* $P < 0.001$).

Figure 9

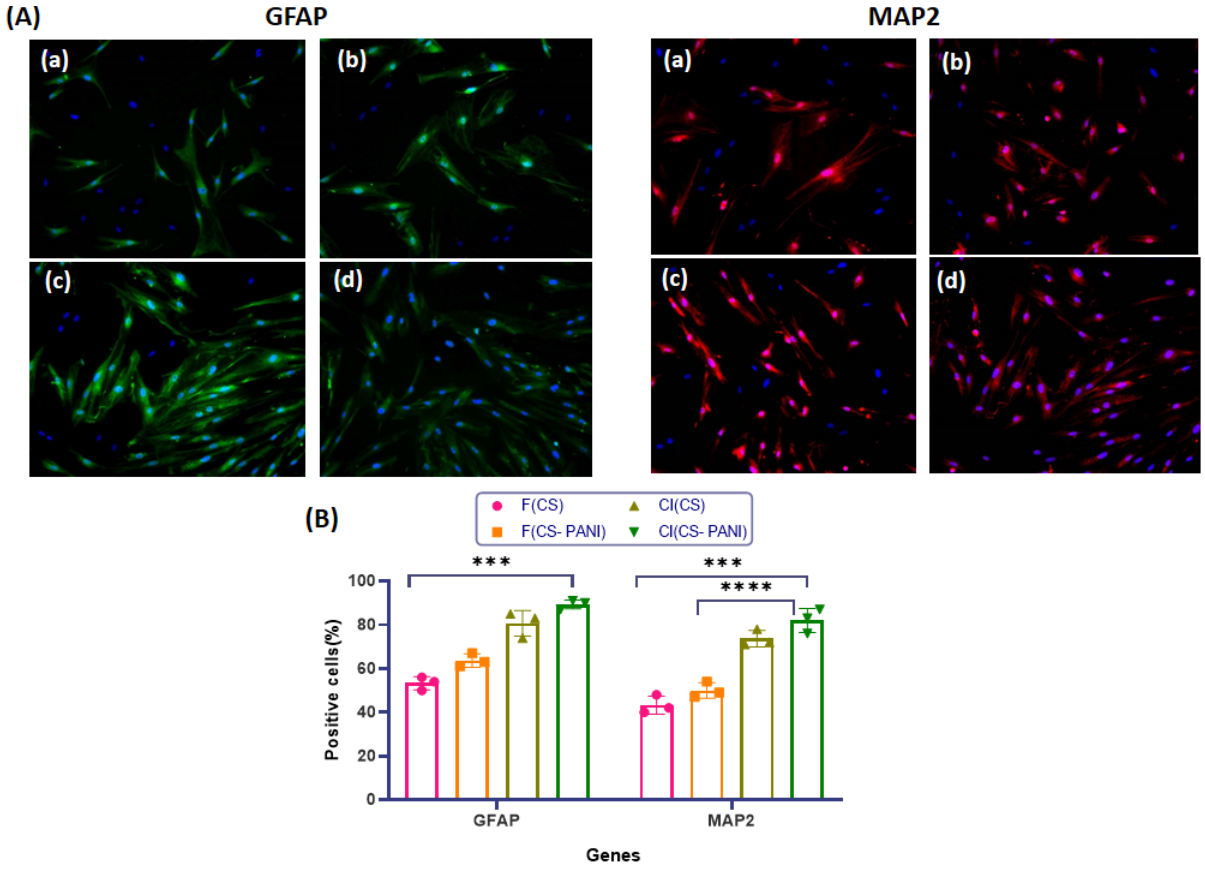

Figure 9. (A) Immunostaining of the rat adipose derived stem cell (rADSCs) expression of GFAP (green) and MAP2 (red) markers. Cell nuclei were stained with DAPI (blue). Scale bar: 100 µm. (B) Average percentage of GFAP and MAP2 expressing rADSCs. (a): F(CS); (b): F(CS-PANI); (c): CI(CS); (d): CI(CS-PANI). $p \leq 0.05$ was considered as level of significance. * indicates significant difference.